ATLAS-NOTE-Phys-109

Precision SUSY Measurements at LHC: Point 3*

I. Hinchliffe[a], F.E. Paige[b], E. Nagy[c], M.D. Shapiro[a], J. Söderqvist[d], and W. Yao[a]

[a] *Lawrence Berkeley National Laboratory, Berkeley, CA*

[b] *Brookhaven National Laboratory, Upton, NY*

[c] *Centre de Physique des Particules de Marseille,France*

[d] *Royal Institute of Technology (KTH), Stockholm, Sweden*

Abstract

This paper, which is one of a series, presents detailed studies of mass reconstructions and other measurements in a case study illustrating the power of the ATLAS detector to perform measurements of supersymmetric particle production. A particular point in the parameter space of the Minimal Supergravity inspired model is used. Reconstruction of gluino, sbottom and light squarks and the measurement of neutralino mass differances is shown.

*This work was supported in part by the Director, Office of Energy Research, Office of High Energy and Nuclear Physics, Division of High Energy Physics of the U.S. Department of Energy under Contracts DE-AC03-76SF00098 and DE-AC02-76CH00016 and by the Swedish National Research Council.

1 Introduction

In the framework of the general strategy of ATLAS [1] to explore the SUGRA [5] parameter space we have studied the point 3 which is defined by the following values: $M_0 = 200$ GeV, $M_{1/2} = 100$ GeV, $\tan\beta = 2$, $A_0 = 0$, $\mathrm{sgn}\mu = -$.

The prominent features of this point are: (*i*) the mass of the gluino and the squarks are relatively small, around 300 GeV, resulting in a large SUSY cross section of 1.3 mb, (see Table 1) and in the direct production of the SUSY particles being dominated by gluino and squark production; (*ii*) if the produced squark is heavier than the gluino, it decays frequently into gluino, therefore in a large fraction of the events there is a gluino pair, and in the majority of the events there is at least one gluino in the final state; (*iii*) the gluino in its turn decays predominantly into a b-quark and a $\tilde{b}_L$,with the latter decaying via $\tilde{b}_L \rightarrow \tilde{\chi}_i^{\pm} q$, $\tilde{\chi}_i^0 b$; (*iv*) the charginos and neutralinos decay with a sizeable branching fraction into electrons and muons. Thus,

$$
\begin{array}{l}
\tilde{q} \longrightarrow \tilde{g} + q \\
\quad \hookrightarrow \tilde{b}_L + b \\
\quad\quad \hookrightarrow \tilde{\chi}_1^{\pm} + q \\
\quad\quad\quad \hookrightarrow \tilde{\chi}_1^0 + l^{\pm} + \nu \\
\quad\quad \hookrightarrow \tilde{\chi}_2^0 + b \\
\quad\quad\quad \hookrightarrow \tilde{\chi}_1^0 + l^+ + l^-
\end{array}
$$

Therefore an unambiguous signature of SUSY can be obtained in the multi-lepton/multi-b-quark channels as it was pointed out in earlier studies [5], [6], [7], [8] [9].

The aim of this note is to give more details on this channel. We first discuss the measurement of $M_{\tilde{\chi}_2} - M_{\tilde{\chi}_1}$ from the endpoint of the dilepton mass distribution. We then reconstruct the gluino and sbottom quark in the above decay chain. Then we discuss light squark reconstruction and the extraction of a signal from the direct production of weakly interacting sparticles. The complete set of masses and branching ratio is given in [10]. All of the plots in this note correspond to 1 year of running at " low luminosity" *i.e.* $10 fb^{-1}$.

2 Detailed Measurements

2.1 Measurement of $M_{\tilde{\chi}_2^0} - M_{\tilde{\chi}_1^0}$

Events are selected by requiring:

- A pair of isolated leptons of opposite charge and the same flavor with $p_{T\ell} > 10$ GeV and $|\eta_\ell| < 2.5$;
- At least two jets tagged as b quarks and having $p_t > 15$ GeV and $|\eta| < 2$; a tagging efficiency of 60% is assumed.

The dilepton invariant mass distribution is shown in Figure 1. The dominant Standard Model background is $t\bar{t}$ production, which is quite small because it has smaller color factors

and requires two leptonic decays. This background, as well as the combinatorial background from events with two $\tilde{\chi}$ decays, can be eliminated by calculating the subtracted distribution:

$$\left.\frac{d\sigma}{dM}\right|_{\rm sub} = \left.\frac{d\sigma}{dM}\right|_{e^+e^-} + \left.\frac{d\sigma}{dM}\right|_{\mu^+\mu^-} - \left.\frac{d\sigma}{dM}\right|_{e^+\mu^-} - \left.\frac{d\sigma}{dM}\right|_{e^-\mu^+} .$$

This subtracted mass distribution has a sharp edge at $M_{\ell^+\ell^-} = M_{\tilde{\chi}_2^0} - M_{\tilde{\chi}_1^0}$, enabling this mass difference to be measured with great precision. In view of the enormous size of the event sample, the uncertainty on this measurement will be limited by systematic effects. The large sample of $Z \to \ell^+\ell^-$ decays can be used for calibration both of the mass scale and of the relative e and μ acceptance. The methods employed will be similar to those used by CDF and D0 in their determinations of the W mass [4, 11]. An estimate of 50 MeV for the uncertainty on $M_{\tilde{\chi}_2} - M_{\tilde{\chi}_1}$ should be conservative.

It should be remarked that most of these leptons arise from the decays of $\tilde{\chi}_2$ produced in the decays of gluinos and squarks. This can be seen clearly in Figure 2 which shows the contribution from the direct production of weakly interacting gauginos. The two signals have the same endpoint at $M(\tilde{\chi}_2^0) - M(\tilde{\chi}_1^0)$ and rather similar distributions for the leptons. The only difference is that the gluino signal has more jet activity. This plot illustrates the difficulty in extracting the signal from this direct production (see 2.5 below).

2.2 Gluino and Sbottom Reconstruction

The next step is a reconstruction of the gluino and sbottom masses by combining a dilepton pair near the mass edge with jets. Events are selected that have

- At least two jets, tagged as having a b quark with $p_t > 15$ GeV and $|\eta| < 2$; a tagging efficiency of 60% is assumed;
- A e^+e^- pair with 45 GeV $< M_{\ell^+\ell^-} <$ 55 GeV and no other electrons or a $\mu^+\mu^-$ pair in the same mass range and no other muons in the event.

Since the mass of the lepton pair is near its maximum value, in the rest frame of $\tilde{\chi}_2$ both $\tilde{\chi}_1$ and the $\ell^+\ell^-$ pair are forced to be at rest. The momentum of $\tilde{\chi}_2$ in the laboratory frame is then determined to be

$$\vec{P}_{\tilde{\chi}_2} = \left(1 + M_{\tilde{\chi}_1^0}/M_{\ell^+\ell^-}\right) \vec{P}_{\ell^+\ell^-} .$$

where $M_{\tilde{\chi}_1^0}$ must be assumed (see below). This momentum can be combined with a b-jet to determine $m_{\tilde{b}}$ and a second b-jet to determine $m_{\tilde{g}}$. The b-jet energy and momentum must be corrected for the fact that particles are lost outside the $R = 0.4$ jet cone and for the fact that weak decays produce neutrinos in the jets. In this study, the correction factor was determined using the data generated for LHC Point 5, where the Higgs peak ($h \to b\bar{b}$) is observable. In practice, techniques similar to those of references [12, 13] would be used at LHC.

Figure 3 shows a scatterplot of $m_{\tilde{g}} - m_{\tilde{b}}$ *vs.* $m_{\tilde{g}}$. Projections onto the axes, shown in Figures 4 and 5, have clear peaks. The positions of the peaks determine $m_{\tilde{g}} - m_{\tilde{b}}$ and $m_{\tilde{b}}$ assuming that $M_{\tilde{\chi}_1^0}$ is known. Again, statistical errors are small and the dominant errors will be from the determination of the jet energy scale. A careful jet energy calibration has not

been performed, so the peaks in Figures 4 and 5 are displaced slightly from their nominal values of 277.8 and 20.3 GeV. These systematic errors can be estimated from those currently obtained by CDF and D0 in the determination of the top quark mass [12, 13]. The mass difference $m_{\tilde{g}} - m_{\tilde{b}}$ is insensitive to the assumed $\tilde{\chi}_1^0$ mass while the reconstructed sbottom peak moves.

The dependence of the $\tilde{b}$ mass peak on the assumed value of $M_{\tilde{\chi}_1^0}$ is shown in Figure 6, where $M_{\tilde{\chi}_1^0}$ is varied by $\pm 20\,\mathrm{GeV}$ from its nominal value. In making this plot we have required that the mass difference $M(\tilde{\chi}_2^0 bb) - M(\tilde{\chi}_2^0 b)$ be within 15 GeV of the value where its distribution peaks. This cut removes considerable background as can be seen by comparing the peaks in this figure with that in Figure 4. We estimate

$$M_{\tilde{b}}(\text{measured}) - M_{\tilde{b}}(\text{true}) = 1.5\Big(M_{\tilde{\chi}_1^0}(\text{assumed}) - M_{\tilde{\chi}_1^0}(\text{true})\Big) \pm 3\,\mathrm{GeV}$$

and

$$M_{\tilde{g}}(\text{measured}) - M_{\tilde{b}}(\text{measured}) = M_{\tilde{g}}(\text{true}) - M_{\tilde{b}}(\text{true}) \pm 2\,\mathrm{GeV}$$

The $\tilde{\chi}_1^0$ mass will be determined by a global fit of the SUSY model to all the measurements; see Section 3.

2.3 Light Squark Reconstruction

Light squarks can also be reconstructed at this point using the decay chain $\tilde{q_L} \to \tilde{\chi}_2^0 q$, which has a branching ratio of approximately 10%. There is an enormous background from gluino decays to $\tilde{b}b$, so events must be rejected if there is a b-jet present. We use the ATLAS b-tagging study (see Figure 3.42 of Ref. [1]). At low luminosity this study implies that a tagging efficiency of 90% for b-jets can be achieved at the price of misidentifying 25% of the light quark jets as b-jets. While this mistag rate is not adequate in the cases where a b-tag is required, it implies that 90% of the b-quark jets can be vetoed and 75% of the light quark jets accepted by the same cut. This veto prescription is used in this subsection.

Events are selected as follows:

- At least one jet with $p_t > 125$ GeV and $|\eta| < 2$.
- No b-jets with $p_t > 15$ GeV and $|\eta| < 2$; a vetoing efficiency of 90% is assumed and 25% of non b-jets are assumed to be rejected also.
- An e^+e^- pair with 45 GeV $< M_{\ell^+\ell^-} <$ 55 GeV and no other electrons or a $\mu^+\mu^-$ pair in the same mass range and no other muons in the event.

The reconstruction of the momentum of $\tilde{\chi}_2^0$ is performed using the same method as above by selecting events near the endpoint of the dilepton mass distribution. We assume that the SUGRA [2] model is used to infer the mass of $\tilde{\chi}_1^0$ from the $\tilde{\chi}_2^0 - \tilde{\chi}_1^0$ mass difference. Jets of $|\eta| < 2$ and $p_t > 125\,\mathrm{GeV}$ are now combined with the $\tilde{\chi}_2^0$ and the mass distribution is shown in Figure 7. Even with the 90% vetoing efficiency for $b-$quarks there are a significant number of $b-$jets remaining in this plot. The contribution from the light squarks is shown as the dashed-histogram. If the vetoing efficiency were raised to 95% approximately one-half of the remaining $b-$jets are removed and consequently the peak moves to a larger mass. The

peak shown has contributions from $\tilde{b_L}$ of mass 278 GeV and the light squarks that have mass around 310 GeV. Charge $-1/3$ and $+2/3$ squarks are separated by about 5 GeV in mass; this contributes to the broadening of the peak. That the peak is real can be seen be estimating the combinatorial background as follows. Events are mixed by taking the $\tilde{\chi}_2^0$ momentum from one event and the jet from another; both events satisfying the same selection criteria. The mass distribution obtained in this way is shown as the hatched distribution in Figure 7. Conservatively, we estimate an error of 20 GeV on the average $\tilde{q}_L$ mass from this method.

2.4 Branching ratio of $\tilde{\chi}_2 \to \tilde{\chi}_1^0 \ell^+ \ell^-$

By selecting events with four tagged $b-$jets and either two or four isolated leptons, the product of branching ratios $BR(\chi_2^0 \to \tilde{\chi}_1^0 \ell^+ \ell^-) \times BR(\tilde{b} \to b\tilde{\chi}_2^0 X)$ can be determined. There are 150000 events/10 fb^{-1} with two reconstructed dilepton pairs and four $b-$jets. The backgrounds from non supersymmetric sources are negligible, and again therefore the dominant uncertainties are systematic. Using a value of 3% for the uncertainty on the absolute lepton acceptance, we expect that $BR(\tilde{\chi}_2^0 \to \tilde{\chi}_1^0 e^+ e^-) \times BR(\tilde{b} \to b\tilde{\chi}_2^0 X)$ can be determined to be $(14.0 \pm 0.5)\%$.

2.5 Electroweak Production of Superpartners

At this SUGRA point, sleptons cannot be produced from the decay of strongly interacting sparticles. The production rates are therefore quite small despite the low masses ($m_{\tilde{e}_L} = 215$ GeV, $m_{\tilde{e}_R} = 206$ GeV) as they must be pair produced in Drell-Yan like processes. The heavier charginos and neutralinos are only rarely produced in the decays of gluinos, so again their dominant production mechanism is electroweak. Unlike the case of sleptons, the direct production rate of the lighter charginos and neutralinos is quite large. An attempt has been made to isolate these processes. This is an example of a case where the analysis of a complete SUSY signal is needed. The signals that we are attempting to extract stand clearly above Standard Model backgrounds, but we face the large background from the production of strongly interacting sparticles. As so few events pass the cuts, we generated separate data samples corresponding to the electroweak production of sparticles and reweighted the events appropriately.

Events are selected that have:

- Three isolated leptons a pair of which have opposite charge and the same flavor with $p_{T\ell} > 10$ GeV and $|\eta| < 2.5$;
- No jets with $p_t > 30\,\mathrm{GeV}$ in $|\eta| < 3.0$.

The jet veto is needed to remove gluino and squark initiated events. These events have jets in the central region arising from the decay products of the sparticles and from final state gluon radiation. These events also have jets, approximately uniform in rapidity, from initial state radiation. This latter source is also present in the direct production of charginos, neutralinos and sleptons. Figure 8 shows the dilepton invariant mass distribution of the two leptons that have opposite charge and the same flavor. The number of *generated* events in this plot is not large, but are sufficient to demonstrate that in 10 fb^{-1} of data there will be sufficient

events for a precise measurement. The background events in this plot (corresponding to three generated events) are from $t\bar{t}$ production, the third lepton being from the decay of a b-quark. A stricter jet veto (20 GeV instead of 30 GeV) reduces this background further.

There is an indication of an edge in the mass distribution corresponding to the decay $\tilde{\chi}_2^0 \to \tilde{\chi}_1^0 \ell^+ \ell^-$. The events in this plot are dominated by the production of $\tilde{\chi}_2^0 \tilde{\chi}_1^\pm$ final states whose contribution is shown as the dotted histogram. If two isolated leptons are required and the same plot made the result is that there are more events. There is now a potential background from Drell-Yan production of dilepton events which must be eliminated by a cut on missing $\not{E}_T$ or the angle between the two leptons; the Drell-Yan events are back-to-back while in the SUSY events the leptons arise from $\tilde{\chi}_2^0 \to \tilde{\chi}_1^0 \ell^+ \ell^-$ and are therefore close in angle. The production rates in these two and three lepton final states can be compared and used to provide a powerful argument concerning the origin of the lepton samples and provide an additional constraint on the model since, as we will demonstrate in section 3 [15], the measurements that have been made using the strong production of sparticles fix the model parameters, resulting in a *prediction* for the rates shown in Figure 8.

In principle, the decay $\tilde{e}_L \to \tilde{\chi}_2^0 e$ should be reconstructible by selecting with a least 3 isolated leptons, an oppositely charged pair of which have mass between 45 and 55 GeV. The momentum of $\tilde{\chi}_2^0$ is reconstructed as above and then combined with a third lepton to search for a reconstructed $\tilde{e}_L$. The extraction of this signal is very difficult. The production rate for gauginos provides a serious background that can only be controlled by increasing the number of isolated leptons required. The dominant slepton production process is $\tilde{e_L} + \tilde{\nu}_e$. This can be extracted only by requiring at least *four* isolated leptons from the decay chain

$$\begin{array}{lcl} \tilde{\ell}_L^+ & + & \tilde{\nu}_\ell \\ \downarrow & & \downarrow \\ \tilde{\chi}_2^0 + \ell^+ & & \tilde{\chi}_1^+ + \ell^- \\ \downarrow & & \downarrow \\ \tilde{\chi}_1^0 + \ell^+ + \ell^- & & \tilde{\chi}_1^0 + \ell^+ + \nu \end{array}$$

or alternatively from

$$\begin{array}{lcl} \tilde{\ell}_L^+ & + & \tilde{\nu}_\ell \\ \downarrow & & \downarrow \\ \tilde{\chi}_2^0 + \ell^+ & & \tilde{\chi}_2^0 + \nu \\ \downarrow & & \downarrow \\ \tilde{\chi}_1^0 + \ell^+ + \ell^- & & \tilde{\chi}_1^0 + \ell^+ + \ell^- \end{array}$$

The dominant decay chain $\tilde{\nu}_\ell \to \tilde{\chi}_1^+ \ell$, $\tilde{\chi}_1^+ \to \tilde{\chi}_1^0 +$ jets is killed by the jet veto requirement. The experiment is only feasible at high luminosity.

3 Conclusions

At this point we have demonstrated that several precise measurements can be made:

- $M_{\tilde{\chi}_2^0} - M_{\tilde{\chi}_1^0} = 52.36 \pm 0.05$ GeV,
- $M_{\tilde{g}} - M_{\tilde{b}} = 20.3 \pm 2.0$ GeV,

- $M_h = 68.3 \pm 3$ GeV.

The Higgs mass would, of course, be measured at LEP, with a precision much better than this. However within the SUGRA model the Higgs mass is sensitive to higher order corrections [16] and theoretical errors are therefore dominant. We can also determine the $\tilde{g}$ and $\tilde{b}_L$ masses precisely as functions of the $\tilde{\chi}_1^0$ mass, providing strong constraints on the model. As described above the mass difference $M_{\tilde{g}} - M_{\tilde{b}}$ is insensitive to the mass assumed for $\tilde{\chi}_1^0$. The low value of the Higgs mass is now excluded by LEP [14]. Nevertheless, the studies at this point illustrate the vast potential of the LHC in the cases where the scale of supersymmetry is relatively low. The extraction of the fundamental parameters from the available measurements will be discussed in another note [15]. However, here we will make a few comments on the sensitivity.

Figures 9, 10 and 11 and 12 show the dependence of $M_{\tilde{\chi}_2^0}$, ΔM, $M_{\tilde{g}}$ and $M_{\tilde{b}}$ on $M_{1/2}$, M_0, tanβ and A_0 in the range of the typical error of these parameters. as predicted by the SUGRA model [3]. Most of these observables are sensitive to $M_{1/2}$ (Fig. 9) and tanβ (Fig. 11), whereas M_0 can be constrained only by $M_{\tilde{b}}$ (Fig. 10). None of the observables is sensitive to A_0 (Fig. 12). On the other hand changing the sign of μ the neutralino masses change considerably. In particular, ΔM, the $\tilde{\chi}_2^0 - \tilde{\chi}_1^0$ mass difference becomes 34.5 GeV, and thus the sign of μ can be easily selected by the endpoint of the lepton-pair invariant mass distribution. It is clear from Figures 9–12 that the three precise measurements listed above are sufficient to determine $M_{1/2}$, M_0, and $\tan\beta$ with good accuracy and that A_0 is undetermined. This is indeed what is found by the detailed fits in [15].

We have illustrated, using specific examples, some techniques that can be used to determine masses and branching ratios of sparticles. Some of these quantities were then used to determine the fundamental parameters of the SUGRA model some of which can be determined with great precision.

The work was supported in part by the Director, Office of Energy Research, Office of High Energy Physics, Division of High Energy Physics of the U.S. Department of Energy under Contracts DE–AC03–76SF00098 and DE-AC02-76CH00016. Accordingly, the U.S. Government retains a nonexclusive, royalty-free license to publish or reproduce the published form of this contribution, or allow others to do so, for U.S. Government purposes. One of us (JS) would like to thank the Swedish National Research council for support.

References

[1] ATLAS Collaboration, *Technical Proposal*, LHCC/P2 (1994).

[2] L. Alvarez-Gaume, J. Polchinski and M.B. Wise, Nucl. Phys. **B221**, 495 (1983);
L. Ibañez, Phys. Lett. **118B**, 73 (1982);
J.Ellis, D.V. Nanopolous and K. Tamvakis, Phys. Lett. **121B**, 123 (1983);
K. Inoue *et al.* Prog. Theor. Phys. **68**, 927 (1982);
A.H. Chamseddine, R. Arnowitt, and P. Nath, Phys. Rev. Lett., **49**, 970 (1982).

[3] F. Paige and S. Protopopescu, in *Supercollider Physics*, p. 41, ed. D. Soper (World Scientific, 1986);

H. Baer, F. Paige, S. Protopopescu and X. Tata, in *Proceedings of the Workshop on Physics at Current Accelerators and Supercolliders*, ed. J. Hewett, A. White and D. Zeppenfeld, (Argonne National Laboratory, 1993).

[4] F. Abe, *et al.*, Phys. Rev. Lett.**75**, 11 (1995).

[5] H.Baer, C-H.Chen, F.Paige, X.Tata, Phys.Rev **D53** (1996) 6241 *and references therein*

[6] G.Montarou, S.Muanza, ATLAS Internal Note Phys-No-61, 1995

[7] V.I.Klyukhin, Presentation at the ATLAS SUSY Workshop Stockholm, January 18-19, 1996

[8] S.Muanza, Thèse de l'Université Blaise Pascal de Clermont-Fd, 1966

[9] A. Bartl, J. Soderqvist *et al.*, to appear in *Proceedings of the 1996 DPF Summer Study* (Snowmass, CO, 1996).

[10] I. Hinchliffe *et.al.* ATLAS-NOTE-phys-107.

[11] S. Abachi, *et al.*, FERMILAB-PUB-96-177-E.

[12] F. Abe *et al.*, Phys. Rev. Lett. **73**, 2667 (1994), Phys. Rev.**D52**, 2605 (1995).

[13] S. Abachi *et al.*, Phys. Rev. Lett. **74**, 2632 (1995).

[14] P. Janot at the International Europhysics Meeting, Jerusalem July 1997.

[15] D. Cavalli *et. al.* ATLAS-NOTE-phys-111.

[16] M Carena, M. Quiros and C.E.M. Wagner, Nucl. Phys, B461 (1996),47.

Table 1: The relevant SUSY particle masses at Point 3

Gluino	298.4 GeV
Light squarks	316.7 GeV
$\tilde{b}_L$	274.3 GeV
$\tilde{b}_R$	313.0 GeV
$\tilde{\chi}_2^{\pm}$	272.1 GeV
$\tilde{\chi}_1^{\pm}$	96.4 GeV
$\tilde{\chi}_2^0$	97.0 GeV
$\tilde{\chi}_1^0$ = LSP	44.5 GeV

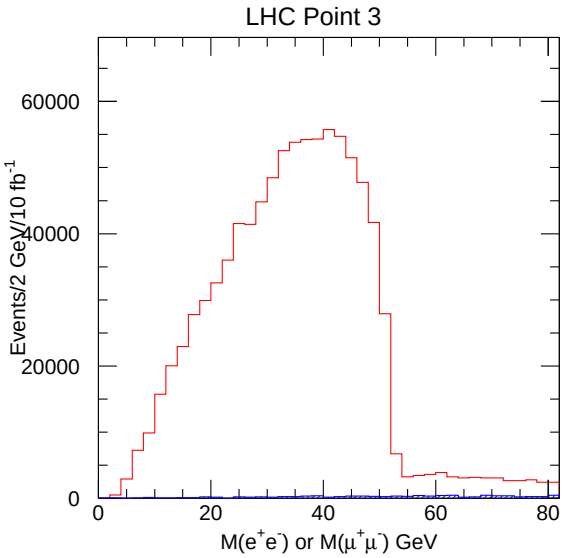

Figure 1: The invariant mass distribution of e^+e^- and $\mu^+\mu^-$ pairs arising at Point 3. The background, shown as a hatched histogram is mainly due to $t\bar{t}$ events.

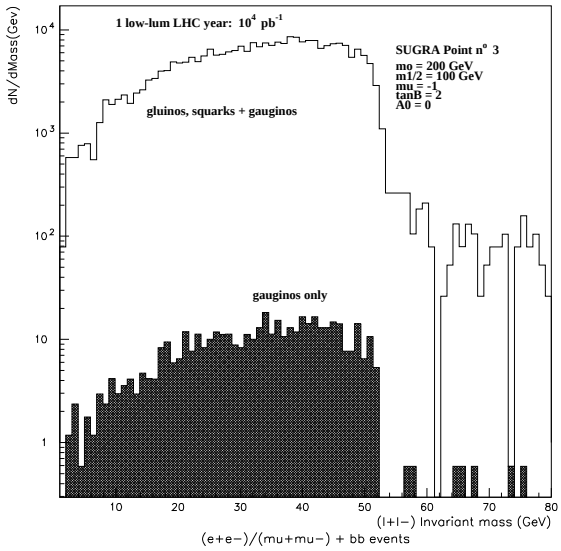

Figure 2: The invariant mass distribution of e^+e^- and $\mu^+\mu^-$ pairs arising at Point 3. The contribution from the direct production of electroweak gauginos is shown as the hatched area. In the latter case, the two $b-$jets arise either from mistagging or from associated production.

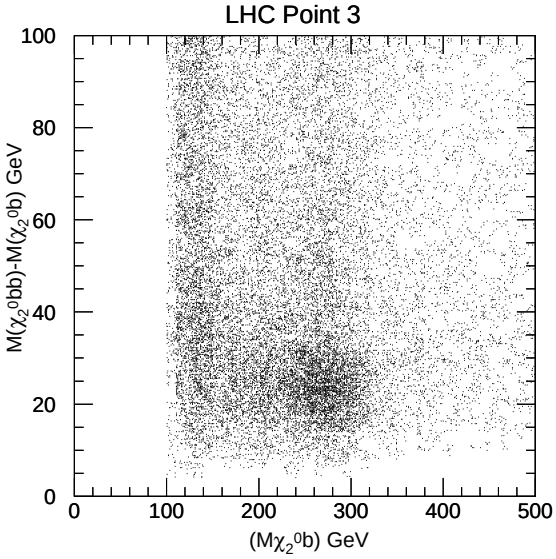

Figure 3: The reconstruction of gluino and sbottom decays from the decay chain $\tilde{g} \to \tilde{\chi}_2(\to \tilde{\chi}_1 \ell^+\ell^-)\tilde{b}$. Events are selected near the endpoint of the $\ell^-\ell^+$ mass distribution (mass between 45 and 55 GeV) and the momentum of $\tilde{\chi}_2$ reconstructed. Two b-jets are then required and the mass of $b + \tilde{\chi}_2$ ($m = m_{\tilde{b}}$) and the mass difference $\delta m = m_{bb\tilde{\chi}_2} - m_{b\tilde{\chi}_2}$ is computed. The scatterplot in these two variables is shown. The b-jet energies have been recalibrated and a tagging efficiency of 60% per b included.

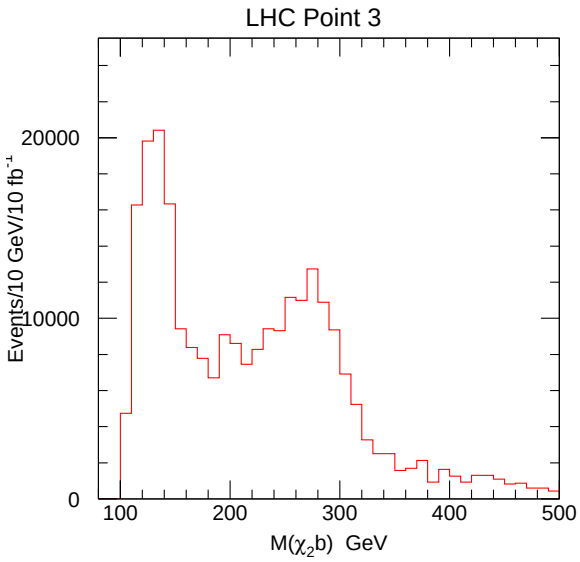

Figure 4: The $M(\tilde{b})$ projection of Figure 3.

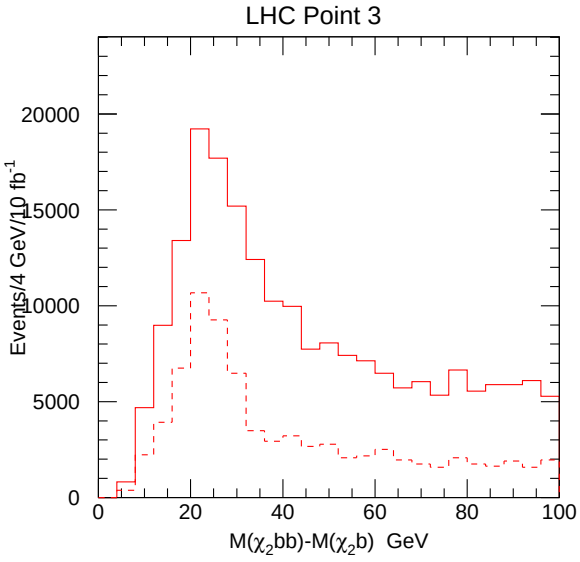

Figure 5: The $M(\tilde{g}) - M(\tilde{b})$ projection of Figure 3. The dashed histogram shows the projection if a cut is made requiring that the events lie in a slice of on the abscissa of between 230 and 330 GeV of Figure 3.

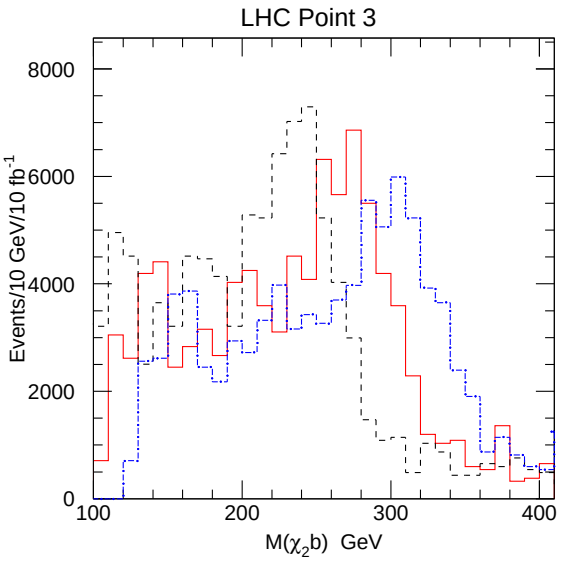

Figure 6: The same as Figure 4 with the addition of two more histograms (dashed and dotted) showing the result if the assumed value of $m_{\tilde{\chi}_i^0}$ is varied by ± 20 GeV. A cut is imposed on the mass difference $|m_{\tilde{g}} - m_{\tilde{b}} - 20|$ GeV < 15 GeV before the projection of the scatterplots is made.

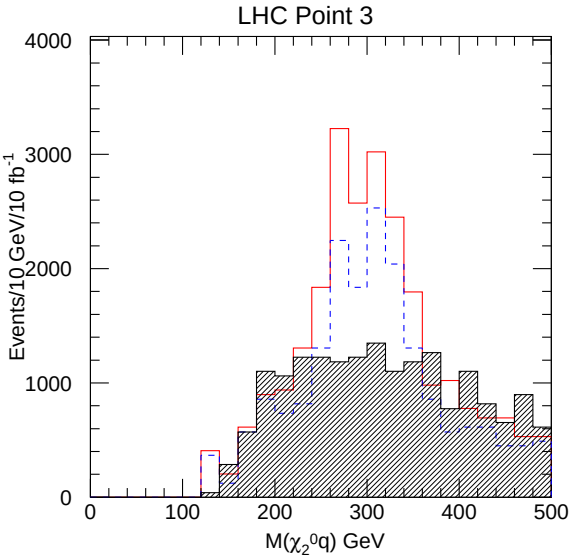

Figure 7: Reconstructed $\tilde{q_L}$ mass at Point 3. The combinatorial background estimate is shown as a hatched histogram and the events due to light squarks as the dashed histogram. The remaining events are due to gluino decays where a b-jet is misidentified as a light quark jet.

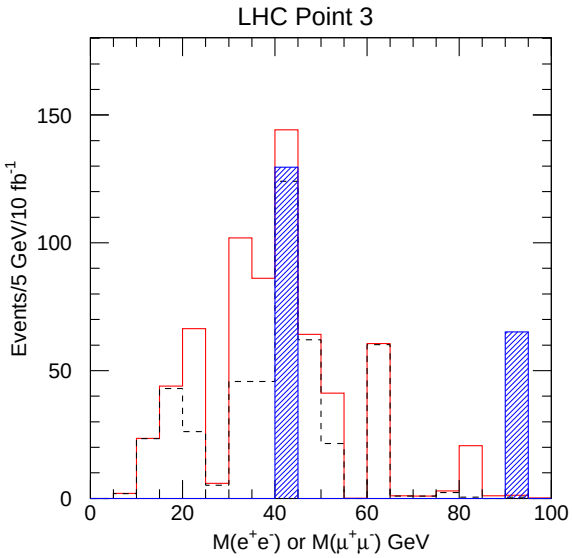

Figure 8: The invariant mass distribution of e^+e^- and $\mu^+\mu^-$ pairs arising at Point 3. Events are selected requiring no jets with $p_t > 30\,\text{GeV}$ in $|\eta| < 3$ and at least three isolated leptons, two of which are of the same flavor and opposite charge. Lepton detection efficiency of 90% per lepton is included. The dashed histogram shows the contribution arising from the direct production of $\tilde{\chi}_1^+\tilde{\chi}_2^0$ final states. The background is shown as the hatched histogram. Only three generated background events passed the cuts.

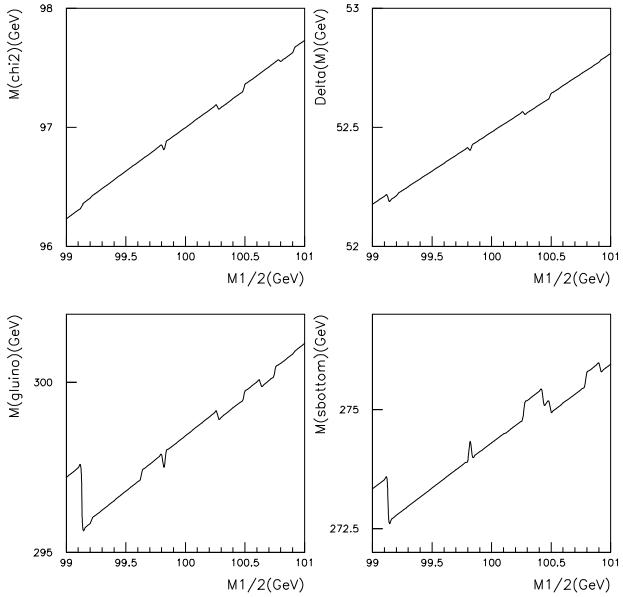

Figure 9: The dependence of $M_{\tilde{\chi}_2^0}$, ΔM, $M_{\tilde{g}}$ and $M_{\tilde{b}}$ on $M_{1/2}$ (the other parameters are fixed at their nominal values).

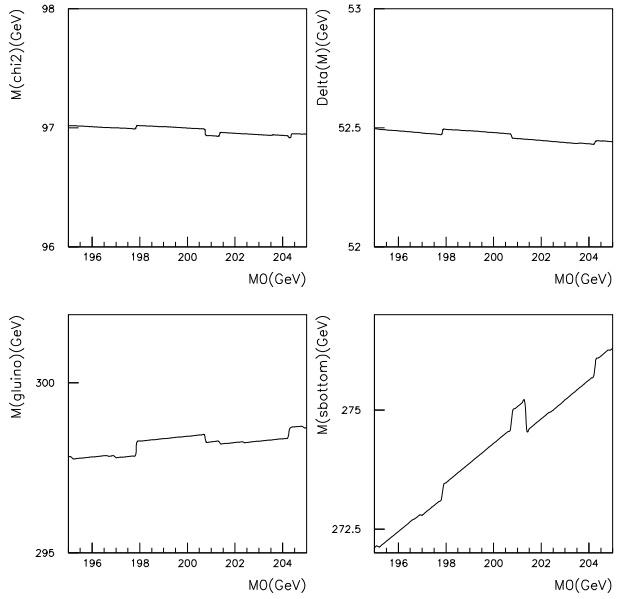

Figure 10: The dependence of $M_{\tilde{\chi}_2^0}$, ΔM, $M_{\tilde{g}}$ and $M_{\tilde{b}}$ on M_0 (the other parameters are fixed at their nominal values).

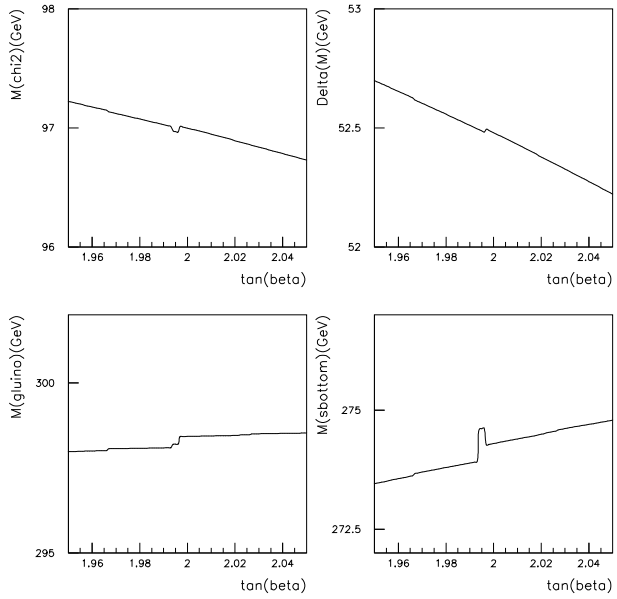

Figure 11: The dependence of $M_{\tilde{\chi}_2^0}$, ΔM, $M_{\tilde{g}}$ and $M_{\tilde{b}}$ on $\tan(\beta)$ (the other parameters are fixed at their nominal values).

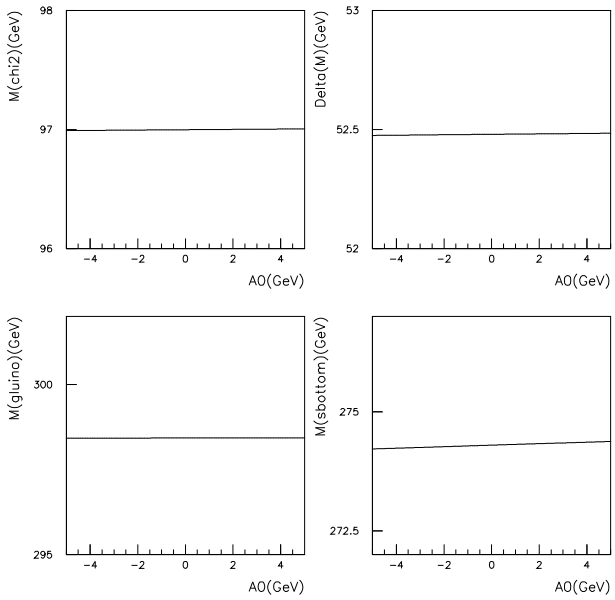

Figure 12: The dependence of $M_{\tilde{\chi}_2^0}$, ΔM, $M_{\tilde{g}}$ and $M_{\tilde{b}}$ on A_0 (the other parameters are fixed at their nominal values).